Far-infrared spectroscopy of halogen-bridged mixed-valence platinum-chain solids: Isotope-substitution studies

S. P. Love, S. C. Huckett, L. A. Worl, T. M. Frankcom, S. A. Ekberg, and B. I. Swanson
Los Alamos National Laboratory, Los Alamos, New Mexico 87545
(Received 7 May 1992)

Far-infrared transmittance measurements are performed on a series of isotopically labeled samples of the quasi-one-dimensional solids $[Pt(en)_2][Pt(en_2X_2][ClO_4]_4$, (en)=ethylenediamine and X=Cl, Br, or I. Pronounced shifts upon deuteration of the (en) ligands reveal that several absorption features previously attributed to localized vibrational modes of chain defects are in fact (en) ligand modes. Recognition of these ligand modes resolves the previous ambiguity over the assignment of the infrared-active chain phonons, permitting the unambiguous assignment of the 238.7-cm^{-1} feature in the bromide material to the asymmetric stretch (ν_2) chain phonon, and strongly suggesting the 184.2-cm^{-1} feature in the iodide is the ν_2 phonon of that material. A high-resolution examination of the chloride, prepared with both natural Cl isotopic abundance and with nearly pure ^{35}Cl, reveals a Cl isotopic fine structure that allows conclusive identification of the 359.1-cm^{-1} feature as the ν_2 chain phonon. Lattice-dynamics calculations using a harmonic-linear-chain model with randomly distributed Cl isotopes yield good agreement with experiment and reveal that isotopic disorder leads to pronounced vibrational localization in PtCl, with the observed fine structure arising from modes residing on a few distinct sequences of isotopes occurring with high probability. The radical difference between the infrared fine structure of PtCl and that previously reported for the Raman-active chain mode is found to result from differences in the dispersion curves for the two phonon branches, and allows indirect determination of these dispersion curves.

I. INTRODUCTION

The *MX* chain solids, consisting of chains of alternating transition-metal complexes and halide ions, have recently been the subject of considerable experimental and theoretical interest because they serve as prototypical low-dimensional charge-density-wave solids.[1-6] Among the most widely studied *MX* solids are compounds of the form $[Pt(en)_2][Pt(en)_2X_2][ClO_4]_4$, where (en)=ethylenediamine-$C_2H_8N_2$ and X=Cl, Br, or I, hereafter referred to by the abbreviations PtCl, PtBr, and PtI. These highly anisotropic, quasi-one-dimensional semiconductors are typically Peierls distorted, with the halide ions displaced from the central position between the metals, and exhibit a concomitant charge disproportionation so that the metals are in alternating valence states best described as a commensurate charge-density wave (CDW). The degree of Peierls distortion and the strength of the CDW can be tuned over a wide range either by varying the chemical composition or through the application of pressure.[7-11] The behavior of these materials at ambient pressure ranges from the highly Peierls-distorted, strong CDW case of PtCl, through the weakly distorted, weak CDW regime of PtI, to the undistorted case of $[Ni(R,R-chxn)_2Br]Br_2$ for which the ground state is possibly a spin-density wave.[12] These materials display clear spectral signatures for various photoinduced electronic gap states (excitons, polarons, bipolarons, solitons),[2,4,6,13,14] and, moreover, have the advantage of being highly crystalline, allowing straightforward interpretation of experimental results.

Because of their versatility and their relative simplicity, *MX* solids are particularly amenable to theoretical modeling, and serve as prototype cases for testing the validity of a given theoretical approach. Recently several treatments of these systems using a Peierls-Hubbard framework have appeared[1,2,5,15-19]. A successful theory should be able to provide a self-consistent description of both the electronic and vibrational properties of these materials. Hence, the frequencies of the fundamental IR- and Raman-active chain phonons provide an important check on the validity of any such model. In addition, considerable theoretical effort has gone into predicting frequencies for the localized vibrational modes associated with intrinsic and photoexcited chain defects such as polarons, bipolarons, excitons, and solitons,[20,21] but a basic knowledge of the ground state vibrational properties of the perfect chain, a necessary starting point for such studies, has been lacking.

The basic structure of the PtX materials[22-27] is illustrated in Fig. 1, which shows two unit cells of the Peierls-distorted PtX chain, as well as the carbon-nitrogen backbones of the planar (en) ligands bound equatorially to each Pt. Not shown, for the sake of clarity, are the hydrogen atoms of the (en) ligands, two of which are bonded to each C and to each N atom, and the ClO_4^- counterions which lie between the chains and complete the crystal structure. If one considers only the one-dimensional $(X—Pt^{III+\delta}—X\cdots Pt^{III-\delta}\cdots)_n$ chain, lattice dynamics[20,21] predicts four in-chain longitudinal photon branches for this four-atom unit cell, three of which are optic modes with nonzero frequency at wave vector $q=0$. At $q=0$, one of these is Raman active and the other two are infrared active.

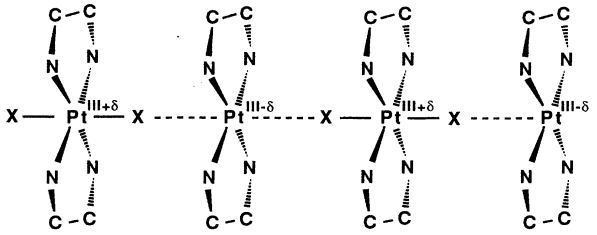

FIG. 1. Basic structure of the $[Pt(en)_2][Pt(en)_2X_2][ClO_4]_4$ chain materials. Shown here is a single Peierls-distorted Pt-X chain, along with the C-N backbones of the (en) ligands, two of which are bonded equatorially to each Pt ion. Not shown, for clarity, are the H atoms of the (en) ligands, two of which are bonded to each C and to each N atom. Also not shown are the ClO_4^- counterions which lie between the chains to complete the crystal structure.

Throughout this article, when discussing lattice-dynamics results for these systems, we shall refer to a simple linear mass-and-spring model for the MX chains, illustrated in the upper portion of Fig. 2, which is essentially the same as used previously by Bulou, Donohoe, and Swanson[20] and similar to that used by Degiorgi *et al.*[21,28] This model assumes harmonic springs and, for simplicity, we define the masses to be simply the Pt and halide atomic masses, leaving out any contribution from the ligands. The first-order approximation using this model is to consider only the nearest-neighbor force constants K_1 (for the $Pt^{III+\delta}$—X interaction) and K_2 (for the $Pt^{III-\delta}\cdots X$ interaction). For better fits to the data, second-nearest-neighbor interactions, K_3 and K_4 (for the two types of X-X interactions) and K_5 (for the $Pt^{III+\delta}$—$Pt^{III-\delta}$ interaction), are included as additional harmonic springs as shown in Fig. 2. Approximate atomic displacements for the three nonzero-frequency $q=0$ modes are shown in the lower portion of Fig. 2. When only nearest-neighbor interactions are considered, the frequency of the Raman mode (ν_1) always falls between that of the upper (ν_2) and lower (ν_3) IR modes.

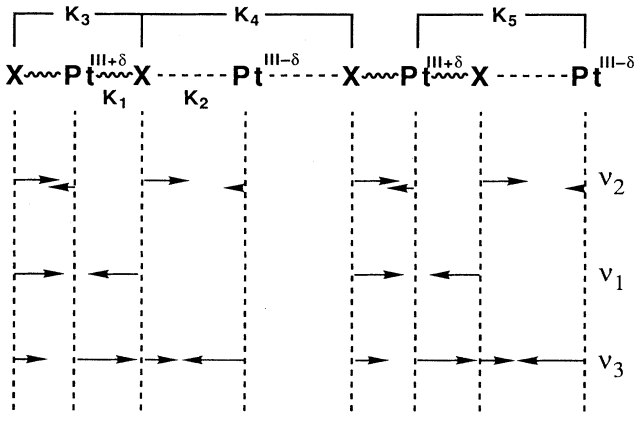

FIG. 2. One-dimensional chain model used for lattice-dynamics calculations. Shown at the top are two unit cells of the Pt-X chain, illustrating the first- and second-nearest-neighbor springs used in this model. The primary force constants are the $Pt^{III+\delta}$—X interaction K_1, and the $Pt^{III-\delta}$—X interaction K_2. Shown below are the eigenvectors for the three zero-wave-vector longitudinal optic chain phonons.

Experimental determination of the frequencies of all three modes would provide information on the strengths of various interatomic interactions within the chain, in particular, the relative stiffness of the $Pt^{III+\delta}$—X and $Pt^{III-\delta}\cdots X$ bonds, and hence the strength of the charge-density wave in each material. Unfortunately, the experimental data available to date has left considerable ambiguity in the assignment of the infrared frequencies. This problem arises partly because early work[28] was performed on impure materials.[22] But the ambiguity lies primarily in the fact that the far-infrared spectra of the real materials include not only the two infrared-active phonons of the chain, but also a host of other absorption features, attributed variously not only to modes involving the ligands and counterions, but also to localized modes associated with defects on the chains themselves. It is clear upon examination of Fig. 1 that the (en) ligands must give rise to numerous IR-active modes, and these must somehow be distinguished from the chain modes of interest if the spectra are to be of any utility in testing theoretical models of these materials. In the past, assignments have typically been made by simply choosing the absorption feature closest in frequency to a theoretical prediction for a given mode. This method may be justified for sufficiently simple spectra, but in the present case, with such a large number of absorption features having similar frequencies and polarization properties, such an approach can easily lead to erroneous assignments. The problem is particularly serious since the ligand modes not included in the theoretical models will most likely couple to the chain modes and perturb their frequencies.

In order to resolve these ambiguities and put the assignment of infrared features on a more rigorous footing, we have performed far-infrared transmission measurements on a series of isotopically labeled PtCl, PtBr, and PtI samples. First, in order to distinguish modes involving substantial motion of the (en) ligands from modes involving motion primarily within the metal-halide chains, the spectra of samples prepared with deuterated (en) ligands are compared to the spectra of undeuterated materials. The results demonstrate that several spectral features previously assigned to chain-defect modes[21] actually involve motion primarily of the (en) ligands. In addition, it is seen in several cases that these ligand modes couple quite strongly to the chain modes, substantially perturbing the chain mode frequencies from what they would be in the case of isolated chains. Through the proper choice of deuteration of the ligands, it is usually possible to shift the ligand modes far from the chain modes, and thus determine chain mode frequencies which more nearly reflect the behavior of isolated chains.

Second, we use isotopic enrichment of the Cl ions in PtCl to unambiguously identify Pt-Cl chain phonons through their isotopic fine structure. We observe that the

359-cm^{-1} feature of PtCl, which had previously been tentatively assigned[21,29] to the Cl—Pt$^{III+\delta}$—Cl asymmetric stretch (ν_2) phonon, actually consists of three closely spaced components. These three components had been observed previously, and it was argued that their relative strengths and positions are consistent with their arising from ^{35}Cl and ^{37}Cl isotopes in their natural abundance,[29] though this assignment remained unproven. Here, preparation of an isotopically pure Pt^{35}Cl sample verifies the isotopic origin of this fine structure, confirms the ν_2 assignment of the 359-cm^{-1} feature, and demonstrates that this vibrational mode, rather than forming extended plane-wave states, is highly localized in PtCl having natural Cl isotopic abundance. The details of this fine structure are of particular interest because they provide, along with our earlier Raman results,[30] direct experimental confirmation of long-standing predictions of intricate structure in the vibrational density of states for one-dimensional systems with isotopic disorder, arising from isotopic "island modes."[31–35] In addition, analysis of the fine structure in the infrared and Raman modes of the isotopically mixed material allows us to indirectly obtain the phonon dispersions for the associated phonon branches in the isotopically pure material.

II. EXPERIMENTAL DETAILS

A. Synthesis

1. *PtX with deuterated ligands*

Pt*X* compounds were prepared with (en) ligands partially deuterated (i.e., $H_2NCD_2CD_2NH_2$, hereafter referred to as d_4-en) and fully deutrated ($C_2D_8N_2$, hereafter referred to as d_8-en), as well as with ordinary undeuterated $C_2H_8N_2$ ligands. The resulting materials shall henceforth be referred to as d_4-Pt*X*, d_8-Pt*X*, and Pt*X*, respectively. Synthesis of all the deuterated materials began with isotopically enriched $H_2NCD_2CD_2NH_2$ (lot no. 4413-N, 98.9 at. % D) purchased from MSD isotopes.

The synthesis of d_8-PtCl was based on a standard method for the preparation of PtCl.[36] K_2PtCl_4 (2.0 g, 4.8 mmol) is reacted with d_4-en (0.45 mL, 6.73 mmol) in H_2O (50 ml) for 2.25 h. The resulting yellow Pt(d_4-en)Cl_2 was filtered, washed with H_2O, and suspended in H_2O (50 mL). To the stirred suspension, d_4-en (0.4 mL, 6.73 mmol) was added and the solution heated to 70 °C at which point it became colorless. From the filtered solution the Pt(d_4-en)$_2Cl_2$ was isolated and half of it dissolved in H_2O, oxidized with Cl_2 and combined with a solution of the remaining Pt(d_4-en)$_2Cl_2$. d_4-PtCl was precipitated by dropwise addition of $HClO_4$ (60%). Dissolving and recrystallizing the d_4-PtCl in D_2O produced the d_8-PtCl; this was performed in a glove bag under Ar and the product stored in a dessicator.

Ordinary and deuterated PtBr were prepared via a route analogous to the PtCl case,[22] beginning by reacting K_2PtBr_4 with either (en) or (d_4-en) to produce Pt(en)$_2Br_2$ or Pt(d_4-en)$_2Br_2$, half of which is then oxidized with Br_2 and reacted with the remaining half to form PtBr. For the deuterated case, some of the d_4-PtBr was collected at this point for spectroscopic study; the remainder was dissolved and recrystallized in D_2O to produce d_8-PtBr. As was recently shown,[22] this synthetic route avoids the problem of Cl contamination which plagued early studies of PtBr.

Two methods were used to synthesize the PtI materials; the products of the two routes were determined to be identical. Both begin with Pt(en)$_2Cl_2$ or Pt(d_4-en)$_2Cl_2$ prepared as described above. In the first method, Pt(en)$_2Cl_2$ is oxidized with I_2 and the resulting solution of [Pt(en)$_2I_2$]Cl_2 reacted with Pt(en)$_2Cl_2$; PtI is then precipitated by dropwise addition of 60% $HClO_4$ and recrystallized from H_2O (or D_2O for the d_8-PtI case). In the second method Pt(en)$_2$(ClO_4)$_2$ is produced by reaction of Pt(en)$_2Cl_2$ with excess $AgClO_4$. Half the Pt(en$_2$(ClO_4)$_2$ is then oxidized with I_2 and reacted with the remaining half, and the product precipitated and recrystallized as in the first method. For the spectra displayed in this article the d_8-PtI was prepared by the first method and the undeuterated PtI was produced by the second.

2. *^{35}Cl-enriched PtCl*

To synthesize ~99% ^{35}Cl enriched Pt^{35}Cl, unenriched PtCl is first prepared as described above. The red crystalline solid (0.05 g, 0.045 mmol) is then dissolved in H_2O (5 mL) and stirred with Na^{35}Cl (0.26 g, 4.5 mmol) obtained from Oak Ridge National Laboratory, until the Na^{35}Cl dissolves. The solution is then covered and maintained at 40 °C for 6 days to ensure thorough Cl exchange. After cooling to room temperature, $HClO_4$ (~2 mL) is added dropwise to precipitate red needle-shaped crystals which are redissolved in H_2O and recrystallized by evaporation over 4 days at 40 °C to produce crystals up to 20×2×1 mm^3.

B. Far-infrared measurements

Pressed pellets of Pt*X* in polyethylene are used for the far-infrared transmission measurements. To fabricate these, the crystals are crushed into a fine powder, mixed with polyethylene powder (90-mg polyethylene to 10-mg PtCl or PtBr; 80-mg polyethylene to 20-mg PtI), heated to 90 °C to soften to the polyethylene, and pressed into 1.6-cm-diam, 0.05-cm-thick pellets, with a resulting volume fill fraction of Pt*X* in polyethylene of roughly 4% for PtCl and PtBr, and 7% for PtI. One exception to these fill fractions is the d_8-PtCl sample, for which there was insufficient material; the fill fraction for the d_8-PtCl pellet is roughly 2%.

In order to ascertain whether the grinding, heating, and pressing involved in the above process introduce strains of magnitude sufficient to produce observable frequency shifts in the infrared modes, a second type of mull sample involving no heating, pressurization, or grinding was made for PtCl. For this second type of sample, small crystallites of PtCl, obtained by rapid precipitation from solution rather than by grinding larger crystals, are mixed with Apiezon "*N*" grease, and the resulting suspension sandwiched between layers of 90-μm-thick po-

lyethylene film. Samples of this second type are generally of poor optical quality, necessitating long integration times when obtaining spectra, but apart from this, their spectra are virtually indistinguishable from those of the pressed pellets, verifying that the pressed pellet spectra are indeed good representations of unstrained material.

The samples are cooled to approximately 20 K in an Air Products Displex closed-cycle helium cryostat equipped with polyethylene windows. Far-infrared spectra from 50 to 500 cm^{-1} are obtained with a Bruker Fourier transform interferometer operating at a resolution of 0.25 cm^{-1} for the PtCl measurements, and at 1.0 cm^{-1} for all other samples. A globar source and room-temperature DTGS pyroelectric detector are used throughout. A pure polyethylene pellet, of the same thickness as the pellets containing the *MX* materials, is used as a reference for all spectra.

III. RESULTS AND DISCUSSION

A. Natural isotope materials: Consideration of small-particle effects and comparison to previous work

The use of transmission measurements on powdered samples suspended in a transparent medium, rather than reflectivity measurements on single crystals, raises the question of the exact nature of the modes responsible for the observed transmission minima, and the degree to which they correspond to the transverse-optic modes of interest. The problem of infrared absorption by optic modes of small dielectric particles has received extensive experimental and theoretical consideration.[40,41] The general result of these studies is that, in the limit of particle dimension much smaller than the wavelength, the observed absorptions are due not to the bulk transverse-optic (TO) phonons, but to small-particle "surface modes" whose frequencies always lie between the TO and longitudinal-optic (LO) frequencies. For typical three-dimensional materials having a large LO-TO splitting, the discrepancy between the small-particle mode frequency and the TO frequency can be substantial, often tens of cm^{-1}.

For the chain phonons of the quasi-one-dimensional *MX* materials, however, the discrepancy between the small-particle mode and bulk TO frequencies should be extremely small, because the very weak interchain coupling will lead to negligible LO-TO splitting. That this intuitive argument is correct can be seen first from the extremely sharp reflectivity peaks reported in Ref. 21 (the reflectivity maximum should extend, at a roughly constant value, from ω_{TO} to ω_{LO}). Secondly, it can be seen from the excellent agreement between frequencies of the major peaks in our small-particle spectra for the case of natural isotopes, Figs. 3(a), 4(a), and 5(a), and those obtained from the single-crystal reflectivity spectra of Ref. 21. In contrast to the chain modes, it is not obvious intuitively that modes involving motion primarily of the ligands (as identified below through ligand deuteration studies) should also have small LO-TO splitting; nevertheless, this appears to be the case, as evidenced again by their very sharp reflectivity peaks, and by the negligible differences in frequency for these features between the small-particle and bulk spectra.

Thus, for these materials, the main disadvantage of the use of pressed pellets is that polarization information is

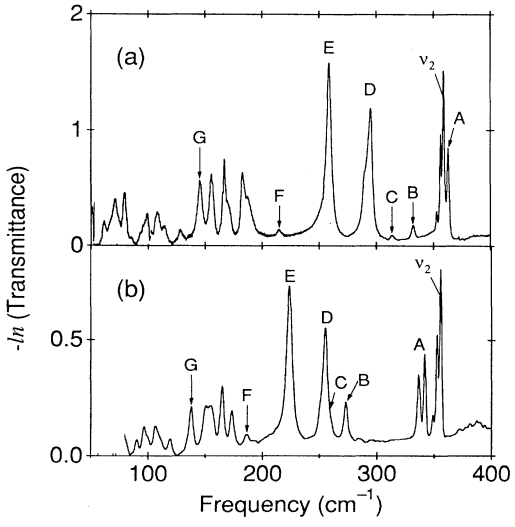

FIG. 3. Far-infrared spectra of PtCl. (a) PtCl prepared with undeuterated (en) ligands. (b) PtCl prepared with fully deuterated d_8-(en) ligands. The three-peaked structure labeled ν_2 is the Cl-Pt-Cl asymmetric stretch chain mode. Features labeled with capital letters $A-G$ are ligand modes which also appear in the PtBr and PtI spectra of Figs. 4 and 5. The region below 80 cm^{-1} is omitted in (b) because of poor signal to noise due to the small amount of d_8-PtCl available. The spectral resolution is 0.25 cm^{-1} in (a) and 1.0 cm^{-1} in (b).

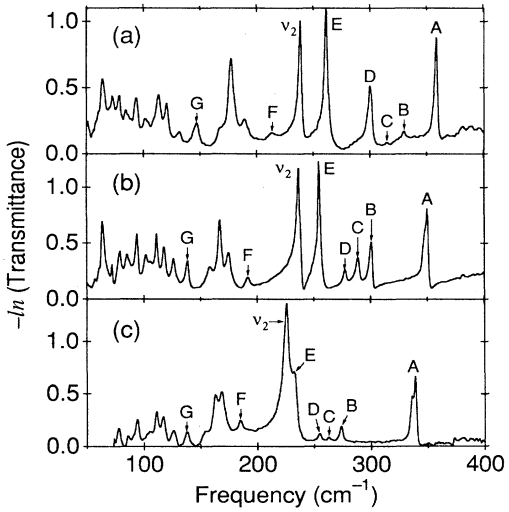

FIG. 4. Far-infrared spectra of PtBr. (a) PtBr prepared with undeuterated (en) ligands. (b) PtBr prepared with d_4-(en) ligands. (c) PtBr prepared with fully deuterated d_8-(en) ligands. The spectral resolution is 1.0 cm^{-1}. Features labeled with capital letters $A-G$ are ligand modes also appearing in the PtCl and PtI spectra of Figs. 3 and 5.

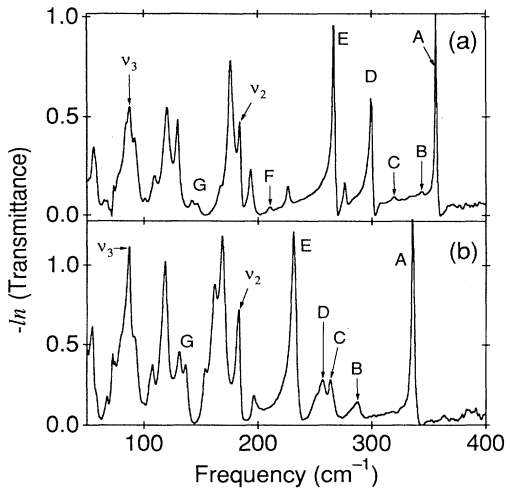

FIG. 5. Far-infrared spectra of PtI. (a) PtI prepared with undeuterated (en) ligands. (b) PtI prepared with fully deuterated d_8-(en) ligands. The spectral resolution is 1.0 cm^{-1}. Features labeled with capital letters $A-G$ also appear in the PtCl and PtBr spectra of Figs. 3 and 4. The feature labeled ν_3 is our best tentative assignment; the feature at 129.7 cm^{-1} is the other reasonable candidate for ν_3 (see text).

lost. The polarizations of the dominant features in undeuterated PtCl, PtBr, and PtI, however, have already been determined in the single-crystal reflectivity work of Ref. 21. Thus, for the natural isotope materials, the present work with its higher effective resolution (small-particle transmission minima tend to be sharper than the corresponding bulk reflectance features), and the single-crystal reflectivity work serve as complementary experiments, which taken together provide a detailed picture of these systems. The good agreement between the two experiments also provides further confirmation that no substantial damage to the crystallites is sustained during the pellet pressing process.

B. Deuteration of the (en) ligands

Figures 3–5 display the far-infrared transmission spectra of PtCl, PtBr, and PtI, respectively, each prepared with undeuterated (top spectrum in each case) and fully deuterated (en), i.e., d_8-(en), ligands (bottom spectrum). In addition, a spectrum for PtBr prepared with partially deuterated (en) ligands, i.e., d_4-(en), with only those four hydrogens attached to the carbon atoms replaced by deuterium, is also shown. We note that the spectrum for undeuterated PtCl in Fig. 3(a) agrees well with that reported earlier by Allen *et al.*[29]

The frequencies of key spectral features observed in this work are summarized in Table I; where appropriate, Table I also notes the frequencies determined by Degiorgi *et al.*[21] for the corresponding features in their chain-polarized bulk reflectance spectra.

The primary goal here is to identify which spectral features arise from vibrational modes of the platinum-halogen chains. To that end, we shall begin by identifying those features which cannot be chain modes.

1. Halogen-independent modes

In order to separate the ligand modes from the chain modes, it is useful to begin by comparing the spectra of PtCl, PtBr, and PtI, noting the common features shared by all three materials. Since changing the halogen species should have a dramatic effect on the frequencies of the fundamental modes within the chains, features which are halogen independent are most likely to be external ligand or counterion modes unrelated to the chains. Examination of Figs. 3–5 reveals several such halogen-independent features. In order to make the correspondences from one material to another more obvious, Table I is layed out so that such directly analogous features appear on the same row of the table for each material. In order to warrant such placement in the table, not only must the modes in question have similar frequencies, but must also display similar shifts upon deuteration.

The following are the major spectral features shared by PtCl, PtBr, and PtI. The letters in parentheses refer to the corresponding labels in Figs. 3–5.

Prominent in the pressed pellet spectra of the undeuterated materials is a mode (A) near 360 cm^{-1} (363.1, 358.7, and 356.3 cm^{-1}, for PtCl, PtBr, and PtI, respectively). Though this mode is quite strong, it is not observed in the chain-polarized data of Ref. 21, and hence must have a transition dipole moment perpendicular to the chains.

A much weaker mode (B) near 332 cm^{-1}, and another (C) near 313 cm^{-1} are also present in all three materials, but are not apparent in Ref. 21, either because they are too weak to show up in reflectance or because they are not polarized along the chain axis. As will be seen, though quite weak, these modes are important in that they couple to the chain mode in undeuterated PtCl, perturbing its frequency.

Each of the undeuterated materials also displays a strong mode (D) near 300 cm^{-1} (295.3, 300.3, and 299.4 cm^{-1}, for PtCl, PtBr, and PtI, respectively), and another of comparable strength (E) near 260 cm^{-1} (258.5, 261.5, and 267.4 cm^{-1} for PtCl, PtBr, and PtI). These modes are also prominent in the chain-polarized reflectance data of Ref. 21, and hence are known to be polarized along the MX chains.

Near 213 cm^{-1} is a relatively weak feature (F) which also appears in Raman and has previously been assigned[37] to the N-Pt-N deformation mode, i.e., the "umbrella" librational mode of the (en) ligands against the chains, an assignment borne out by the isotope shifts.

Finally, each material displays a mode (G) near 145 cm^{-1} which behaves similarly under deuteration for all three materials. This mode is quite strong in PtCl and PtBr and is also seen in the chain-polarized data of Ref. 21. In PtI, however, it is quite weak and is not apparent in the data of Ref. 21.

2. Isotope shifts of the (en) modes

In this section we shall examine in detail the behavior of the above modes upon deuteration. In considering the isotope shifts of the various modes, it is useful to note, as a benchmark case, that a mode which involves purely

translational motion of (en) as a rigid unit, with no motion of other species, will experience a reduction in frequency by a factor of 1.033 in going from $C_2H_8N_2$ to $C_2D_4H_4N_2$, and by a factor of 1.065 in going from $C_2H_8N_2$ to $C_2D_8N_2$ (i.e., by a factor of the square root of the ratio of the masses). These shifts are the largest that can be expected for purely translation motion of (en), and by this benchmark, it will be seen that all seven of modes $A-G$ discussed above exhibit very substantial shifts upon deuteration and therefore involve primarily (en) motion. Indeed, several of these modes exhibit frequency shifts by factors greater than 1.065, indicating that these modes are not purely translational in character, but must involve libration and/or internal distortion of the (en) units.

Because the spectra are quite complex, making it difficult to follow the deuteration shifts for all modes in a single material, it is often helpful to first examine the behavior of a particular mode in a material for which there are no other modes in the vicinity to confuse the picture, then compare the behavior of the corresponding feature in the other materials. Thus, the effects of deuteration on

TABLE I. Compilation of far-infrared peak frequencies for PtCl, PtBr, and PtI with (en), d_4-(en), and d_8-(en) ligands. All frequencies are in cm^{-1}. Placement of some features in the same row in this table is meant to suggest these features arise from analogous modes. Assignments with question marks are tentative, and in the case of PtI ν_3 two possibilities are given (see text).

PtCl			PtBr				PtI			
(en)			(en)				(en)			
This work	Ref. 21	d_8-(en)	This work	Ref. 21	d_4-(en)	d_8-(en)	This work	Ref. 21	d_8-(en)	Assignment or label
363.1		341.9	358.7		350.5	339.0	356.3		335.6	(en) mode *A*
		336.6				336.0				
359.1	(359)	355.8								PtCl ν_2
356.5[a]		352.5[a]								PtCl ν_2
352.9[a]		348.8[a]								PtCl ν_2
332.3		273.5	330.3		301.0	273.9	343.8		287.4	(en) mode *B*
313.8			314.8		289	262.8	319.7		263.8	(en) mode *C*
295.3	(294)	255.2	300.3	(298)	278	255.0	299.4	(298)	257.0	(en) mode *D*
258.5	(258)	224.0	261.5	(266)	255	232.5	267.4	(266)	231.4	(en) mode *E*
			238.7	(238)[b]	237	226.1				PtBr ν_2
214.9		186.6	213.5		191.4	185.1	210.7		183.1	(en) mode *F*
							184.2	(186)	183.1	PtI ν_2
187.4		173.4	189.1		175.0	168.4	193.8		168.8	
183.2		164.9	177.4		167.3	163.0	175.7		162.2	
167.3										PtCl
165.6[a]										bending
163.4[a]										
170		154.8	168.7		158.6	154.8	166.8		154.0	
156.0		150.9								
145.8	(137)	137.9	147.0	(145)	138.9	138.0	146.6		136.9	(en) mode *G*
							142.0		131.1	
			131.3		126.3	126.3				
128.5		119.6					129.7	(129)	118.6	PtI ν_3 (?)
120.8		118.0	117.0	120.1						
			113.3		111.4	111.0				
108.3		106.8					109.7		107.5	
		101.7	102.0		102					
96.6		96.7								
			94.0	(96.8)	94.0	94.5				
							87.3	(88.7)	87.0	PtI ν_3 (?)
			84		85	85				
			79		79	79				
			63.6		63.6					
77.2										
68.6										
59.1										

[a]Does not appear in pure ^{35}Cl materials.

[b]Reference 21 tabulates a value of 28 meV (226 cm^{-1}), but direct examination of their spectrum indicates a value of approximately 29.5 meV (238 cm^{-1}). See text.

mode A can perhaps be most easily understood by first examining the spectra for PtBr and PtI.

In PtBr, mode A is seen to shift from 358.7 cm^{-1} for $C_2H_8N_2$ ligands, to 350.5 cm^{-1} for $C_2D_4H_4N_2$ ligands (a factor of 1.023), while at the same time showing a slight splitting into two modes. With $C_2D_8N_2$ ligands, the splitting becomes obvious, with the stronger component appearing at 339.0 cm^{-1}, a shift by a factor of 1.058 from the undeuterated case. In PtI, the 356.3-cm^{-1} mode undergoes a similar shift upon full deuteration (by a factor of 1.062) but no splitting is apparent.

With the behavior of mode A established, the deuteration shifts in the rather congested $\sim$360-cm^{-1} region of PtCl become clear. Here mode A is the feature at 363.1 cm^{-1} in the undeuterated material, which upon deuteration shifts (by a factor of 1.062) and splits into two components in a manner similar to that seen for PtBr, albeit with somewhat greater splitting. The remaining three-peaked structure, which undergoes only a very small shift upon deuteration, arises from the Cl-Pt-Cl asymmetric stretch mode of the chains (ν_2), as discussed below.

In all three materials, the weak modes B and C undergo large shifts upon deuteration, and couple strongly to each other and to mode D in the deuterated materials, resulting in substantial redistribution of oscillator strength among the three modes. Thus, the three features observed for the deuterated case arise from modes which are not precisely the same as in the undeuterated case, as implied by the labeling in the figures, but which instead have strongly mixed character.

Mode E, the strong feature near 260 cm^{-1}, shifts down by a factor of 1.156 upon deuteration in both PtCl and PtI. In PtBr, however, mode E couples to another strong mode, at 238.7 cm^{-1} in the undeuterated material, which has a much weaker isotope shift. The result is that mode E shifts only by a factor of 1.125 in PtBr, while the 238.7-cm^{-1} mode is forced to shift by a greater amount than it would were mode E not present.

The authors of Ref. 21 suggest that mode E, which appears in their chain-polarized reflectance spectra, is a localized out-of-chain bending mode associated with polaron defects on the MX chains. The large isotope shift of mode E, as well as its large dipole strength (comparable to or greater than that of the fundamental antisymmetric stretch chain phonon for all three materials) and its presence in all three materials at roughly the same frequency, strongly refute this assertion.

The present data show, rather, that mode E primarily involves large-amplitude motion of the (en) ligands. The sequence of PtBr spectra gives additional clues to the nature of this mode. It is seen that in going from $C_2H_8N_2$ to $H_2NCD_2CD_2NH_2$ ligands, mode E undergoes a relatively small shift, by a factor of 1.026, while a much larger shift by a factor of 1.097, occurs in going from $H_2NCD_2CD_2NH_2$ to fully deuterated ligands. Thus, it appears that mode E involves considerably larger-amplitude motion of the nitrogen atoms and their associated hydrogens than it does of the carbon atoms. Since it is known from structural studies that each of the Pt atoms on the chains are coordinated by the four N atoms of two (en) ligands, with the C atoms of the (en) located considerably farther away from the Pt atoms (see Fig. 1), this large-amplitude nitrogen motion is inconsistent, for example, with libration of the (en) as a rigid unit about a Pt pivot. Instead, it appears that mode E must involve internal distortion of the (en) unit, with large out-of-plane movement of the N atoms.

The deuteration shifts of mode F near 213 cm^{-1}, in contrast, are consistent with quasirigid libration of the (en) with the Pt atoms as a pivot point. Examining the PtBr data again, we see that in going from undeuterated to (d_4-en) ligands mode F shifts by a factor of 1.116, while in going from (d_4-en) to (d_8-en) ligands it shifts further only by a factor of 1.034, consistent with a larger-amplitude motion for the carbon side of the (en) molecule than for the nitrogen side, which arises quite naturally since the nitrogens are closer to the axis of libration. This observation is in accord with a previous assignment[37] of a Raman feature at this same frequency to this (en)-Pt-(en) "umbrella" mode.

Finally we note that mode G near 145 cm^{-1} undergoes a substantial shift on deuteration, by factors of 1.057, 1.058, and 1.071 in PtCl, PtBr, and PtI, respectively, comparable to that predicted for rigid translation of (en). This, then, is clearly another ligand mode. [The somewhat larger shift in PtI raises the question of whether the PtI feature is actually the same mode as in PtCl and PtBr; nevertheless, its primarily (en) character is quite clear.] Reference 21 assigns this feature to the lower-frequency IR-active chain mode, ν_3, in PtCl, and to a localized gap mode associated with polaron defects on the MX chains in PtBr. The present data do not support either of these assignments.

C. Chain modes

We now turn to the identification of the chain modes, which are the primary interest of this work. In the preceding section, several strong features were noted, which unlike the ligand modes, are unique to each PtX compound and have frequencies which are quite immune to the effects of deuteration of the (en) ligands. These include the three-peaked structure in PtCl (359.1, 356.5 and 352.9 cm^{-1} in the undeuterated material), the PtBr mode which falls at 238.7 cm^{-1} in the undeuterated material, and the 184.2-, 129.7-, and 87.3-cm^{-1} modes in PtI. All of these modes are polarized along the chains, as evidenced by the fact that they also appear in the chain-polarized reflectance spectra of Ref. 21. In this section we shall discuss how the present work provides evidence for the assignment of these features to chain phonons. Of particular interest is the Cl isotopic fine structure observed for PtCl. We shall present lattice-dynamics calculations which show that this fine structure is the result of vibrational modes which become highly localized due to the isotopic disorder. In addition, we shall point out the cases for which previous assignments appear to be in error or for which the available experimental data still leave ambiguities.

1. PtCl ν_2

The present results show conclusively not only that the $\sim$359-cm^{-1} feature arises from the Cl—$Pt^{III+\delta}$—Cl

asymmetric stretch mode (ν_2) of the chains, as was suggested in Refs. 21 and 29, but also that its three-peaked fine structure (359.1, 356.5, and 352.9 cm^{-1} in the undeuterated material and at 355.8, 352.5, and 348.8 cm^{-1} in the deuterated case) arises from Cl isotopes. Figure 6 shows an expanded view of the $\sim$360-cm^{-1} region of PtCl for three different isotopic labelings: Figure 6(a) displays the spectrum for ordinary, undeuterated PtCl with natural Cl isotopic abundance, while Fig. 6(c) shows the spectrum for PtCl (natural Cl isotopic abundance) with deuterated (en).

The isotopic origin of this fine structure is confirmed in Fig. 6(b), which shows the spectrum for undeuterated PtCl prepared with nearly pure ^{35}Cl. Here the 352.9-cm^{-1} feature becomes too weak to observe and the 356.5-cm^{-1} mode is greatly reduced in strength.

Note that, in addition to the small shifts in frequency, the spacing of the three peaks is somewhat greater in the deuterated case of Fig. 6(c) than in the undeuterated samples. We attribute both the frequency shifts and the compression of the three isotope features in the undeuterated case to coupling with the nearby ligand mode at 332.3 cm^{-1} (mode *B*) and possibly with the ligand modes at 313.8 and 295.3 cm^{-1} (modes *C* and *D*). The effect of this coupling is to push the chain modes up in frequency and the ligand mode(s) down, the effect being stronger the smaller the separation between the interacting modes. In the deuterated samples, the ligand modes shift down far from the chain modes and this coupling is greatly reduced. The ν_2 mode frequencies for the deuterated material are thus probably quite close to what they would be for an isolated chain.

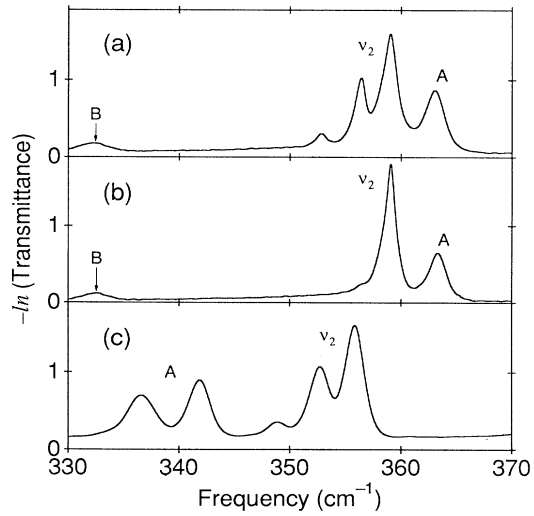

FIG. 6. Far-infrared spectra of PtCl, showing the fine structure in the ν_2 region. (a) PtCl with undeuterated ligands and natural Cl isotopic abundance (75% ^{35}Cl, 25% ^{37}Cl). (b) PtCl with undeuterated ligands, highly enriched ^{35}Cl abundance ($\sim$99% ^{35}Cl). (c) PtCl with natural Cl isotopic abundance, but with deuterated d_8-(en) ligands. The three features arising from the asymmetric stretch chain phonon are labeled ν_2. The features labeled *A* are ligand modes, as in Fig. 3. The spectral resolution is 0.25 cm^{-1} in (a) and (b), and 1.0 cm^{-1} in (c).

2. *Discussion of the PtCl isotopic fine structure*

The isotopic fine structure in the ν_2 mode bears further discussion at this point because it sheds light on the general problem of lattice dynamics in 1D solids, namely, the effects of vibrational localization due to isotopic disorder, and also because examination of this problem raises several points which will be relevant to the interpretation of the spectra for the other *MX* materials.

The fine structure in the ν_2 mode is another manifestation of the vibrational localization, due to the disorder of the Cl isotopes on the chain, which we have recently shown[30] to be responsible for the complex fine structure in the Raman-active ν_1 mode at 311 cm^{-1}, reproduced in Fig. 7(a). What is surprising, however, is the considerable difference between the fine structure in the ν_1 Raman spectrum and that in the ν_2 infrared spectrum. While the ν_1 Raman fine structure in Fig. 7(a) is quite complex, with six distinct peaks and several weaker ones spread over the frequency range from 305 to 316 cm^{-1}, the ν_2 infrared fine structure in Fig. 6 is quite simple, with just

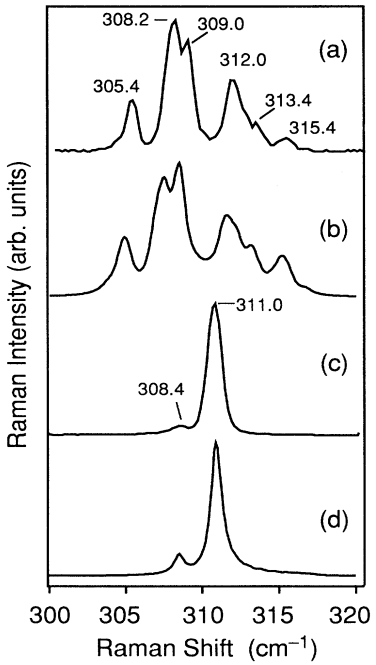

FIG. 7. Experimental and predicted Raman spectra for the ν_1 region of PtCl. (a) Experimentally observed spectrum Raman spectrum for a PtCl single crystal with natural Cl isotopic abundance, obtained at 13 K, using 2.41-eV excitation. Incident and scattered light are polarized parallel to the chain axis. The frequencies in cm^{-1} of the major features are noted in the figure. (b) Spectrum of PtCl with natural Cl isotopic abundance calculated from the harmonic-linear-chain model using the same spring constants as used for the IR results of Figs. 8(d) and 8(e). (c) Experimentally observed spectrum Raman spectrum for a $\sim$99% ^{35}Cl-enriched PtCl single crystal, obtained under the same conditions as in (a). (d) Raman spectrum predicted by the harmonic model for $\sim$99% ^{35}Cl-enriched PtCl, using the same spring constants as in (b).

three peaks with relative strengths very close to the 9:6:1 proportion expected for noninteracting Cl-Pt-Cl molecules with the Cl isotopes in their natural abundance of 75% ^{35}Cl and 25% ^{37}Cl. Indeed, if one considers the asymmetric stretch mode for a simple harmonic mass-and-spring model of an isolated Cl-Pt-Cl molecule and computes the spring constant from the 355.8-cm^{-1} ^{35}Cl-Pt-^{35}Cl mode of the deuterated material, one calculates frequencies of 352.5 and 348.7 cm^{-1} for the ^{35}Cl-Pt-^{37}Cl and ^{37}Cl-Pt-^{37}Cl asymmetric stretch modes, respectively, in excellent agreement with the observed values. In contrast, this local oscillator model fails to even qualitatively predict the Raman results.

The complexity of the Raman fine structure has led to considerable confusion over the years. The noninteracting $PtCl_2$ molecule model for the PtCl chains was first proposed by Allen *et al.*[29] and Clark and Croud[38] at a time when only low-resolution Raman data on powdered samples was available. In these early spectra the complex ν_1 fine structure merged into three broad peaks, which those authors argued was in accord with their model. But instead of the expected 9:6:1 intensity ratio, the central peak was observed to be strongest. This discrepancy placed doubt on the Cl isotope explanation for the Raman fine structure. Subsequent single-crystal, higher-resolution measurements by Tanaka and Kurita[39] revealed not three but five components to the ν_1 fine structure, with the two new features falling at *higher* frequency than the mode previously attributed to the lightest isotopic combination, ^{35}Cl-Pt-^{35}Cl. This led Tanaka and Kurita to completely reject the Cl isotope explanation for the fine structure and to propose an entirely different mechanism. They suggested that, instead of crystallizing into long perfect chains, the PtCl chains were highly disrupted, forming short chain segments delineated by defects. Each of the fine-structure components was argued to be associated with a particular length of segment, with the intensities reflecting a preferred distribution of lengths. This explanation, if correct, would have meant that PtCl would have severely limited usefulness as a prototype one-dimensional (1D) solid. While the isotope enrichment results presented here and in Ref. 30 show conclusively that the fine structure in ν_1 as well as in ν_2 does after all result from Cl isotopes, the primary insight gained is that it is the *disorder* of those isotopes and the resulting *localization* of the vibrational modes which are the key factors.

In order to elucidate the role of isotopic disorder and the factors responsible for the unexpected difference between the isotopic fine structure of the IR-active ν_2 mode and that of the Raman-active ν_1 mode, we present in this section results of lattice-dynamics calculations on linear PtCl chains with randomly distributed ^{35}Cl and ^{37}Cl isotopes. These results show that the observed fine structure arises from vibrational modes localized on short chain segments or "islands" defined by a few specific sequences of ^{35}Cl and ^{37}Cl isotopes occurring with high statistical probability. We shall see that although the isotopic sequences which give rise to the various ν_1 Raman peaks are the same as those which produce the ν_2 infrared fine structure, the detailed pattern of frequencies and intensities of the various peaks is very different for the two cases, contrary to what one might intuitively expect, because the localized modes depend critically on the magnitude and direction of the dispersion of their associated phonon branches.

To understand how this arises, it is useful before proceeding to the calculations to recall the well-known result that substitutional mass defects give rise to new vibrational modes localized at the defects.[35] For a two-component chain, substitution for the lighter component (Cl in this case) gives rise to either a local mode above the optic branch or to a gap mode below it, depending on whether the substituted atom is lighter or heavier than the original, respectively. In both cases, the degree of localization increases with the mass difference between the substituted and original atoms. Localized modes associated with each of the optic branches, ν_1, ν_2, and ν_3, should occur in the present case. The local mode evolves out of the highest optic phonon in the branch (at the Brillouin zone boundary for ν_1 and zone center for ν_2) while the gap mode evolves from the lowest (zone center for ν_1 and zone boundary for ν_2), and they retain some of those phonons' character if the substituted atom is close in mass to the original.

At this point, the role of the dispersion of the phonon branch in dictating the localized mode frequencies is already clear: Since the local mode must lie above the highest phonon in the associated optic branch and the gap mode must lie below the lowest phonon in the branch, the greater the dispersion of that branch, the greater the spread of localized mode frequencies.

These ideas can easily be applied to the highly enriched Pt^{35}Cl case since it can be thought of as perfect Pt^{35}Cl chains with dilute ^{37}Cl defects. With the Peierls distortion of the PtCl chains, it is more natural in this case to think in terms of substituting Cl-Pt$^{III+\delta}$-Cl units rather than single Cl atoms; we shall abbreviate these units by referring only to the Cl isotopes surrounding the Pt$^{III+\delta}$ (e.g., a "35-37 unit"=^{35}Cl-Pt$^{III+\delta}$-^{37}Cl). It is clear that the strong 359.1-cm^{-1} feature is the zone center ν_2 phonon for a nearly perfect Pt^{35}Cl chain, while the weak 356.5-cm^{-1} feature is the gap mode arising from 37-35 defects (for the d_8-PtCl case, which, as discussed in the preceding section, is probably a better representation of the isolated chains, the zone center phonon is at 355.8 cm^{-1} and the 37-35 gap mode is at 352.5 cm^{-1}). Similarly, in the Raman spectra,[30] the 37-35 gap mode associated with the 311-cm^{-1} ν_1 phonon falls at 308.4 cm^{-1}.

For PtCl with 25% ^{37}Cl, the extremely high heavy-isotope density means it is no longer entirely appropriate to think in terms of isolated defects on otherwise perfect chains and the situation can become quite complicated. It is here that explicit calculations facilitate further understanding. To simulate spectra of various isotopic mixtures, we calculate the normal mode eigenfrequencies and eigenvectors for a finite chain of the type illustrated in Fig. 2, typically 32 unit cells (128 atoms), with periodic boundary conditions. This is done in the standard manner, by diagonalizing the appropriate dynamical matrix. The formalism we use is essentially the same as that used by Barker and Sievers.[35] Details are given in the

Appendix.

We begin the calculations by adjusting the spring constants so that, for a pure $Pt^{35}Cl$ chain and a chain with a single ^{37}Cl defect, the model yields results consistent with experiment for the 99% ^{35}Cl sample. Once the spring constants have been established for this case, the problem is then solved, using the same springs, for chains with randomly distributed Cl isotopes, in which the occupation of a given site by ^{35}Cl or ^{37}Cl is determined by a random number generator. In order to attain good statistics without diagonalizing inordinately large matrices, we solve 100 128-atom random chains, rather than a single long chain, and combine the results in the simulated spectra. The infrared spectra are simulated by assigning a Lorentzian line shape of fixed width to each normal mode and summing over all modes. The dipole moment for each eigenvector is calculated in a straightforward manner from the atomic displacements, assuming Pt charges of +2 and +4, and a Cl charge of −1 electron. The simulated Raman spectra shown in Fig. 7 are produced in a similar manner, with the Raman intensity for each normal mode estimated by considering only the $Pt^{III+\delta}$—Cl bonds, setting the polarizability change proportional to the change in bond length and summing over all $Pt^{III+\delta}$—Cl bonds.

Demanding that the model agree with experiment for the 99% ^{35}Cl case sets up a number of requirements. The first set of requirements come from our previous work on the Raman fine structure:[30] the zone center ν_1 phonon for the pure $Pt^{35}Cl$ chain must fall at 311.0 cm^{-1}, and the gap mode for dilute 37-35 defects in a $Pt^{35}Cl$ chain must fall at 308.4 cm^{-1}. We showed in Ref. 30 that this second condition requires in effect that the ν_1 branch disperse upward by 6.5 cm^{-1} from zone center to boundary. These two conditions by themselves can be satisfied using just the two nearest-neighbor force constants, and the Raman results could be reproduced quite well (without attempting to fit the IR results) using $K_1=134.6$ and $K_2=66.3$ N/m. Further conditions are imposed by the present IR results—that the zone center ν_2 phonon for the pure $Pt^{35}Cl$ chain falls at 355.8 cm^{-1} and that the 37-35 gap mode falls at 352.5 cm^{-1}. To simultaneously satisfy these and the Raman conditions requires the inclusion of the second-nearest-neighbor interactions, K_3, K_4, and K_5 as in Fig. 2. In Ref. 30, we used the following set of force constants to provide a reasonable fit to both the Raman and IR results: $K_1=165$, $K_2=45$, $K_3=K_4=-2.3$, and $K_5=36$ N/m. The conditions discussed so far, however, do not uniquely determine the set of five force constants and considerable flexibility remains for choosing physically reasonable values.

The effect of the choice of spring constants on the infrared spectrum of a 75% ^{35}Cl, 25% ^{37}Cl material is illustrated in Fig. 8. For each of the simulated spectra in Fig. 8, a set of spring constants was chosen such that the zone center ν_2 phonon for the pure $Pt^{35}Cl$ chain falls at 355.8 cm^{-1}. The difference between the spectra lies in the degree of coupling between adjacent Cl-$Pt^{III+\delta}$-Cl units, determined for the ν_2 mode primarily by the ratio K_2/K_1, and the dispersion of the ν_2 branch, determined by the K_2/K_1 ratio as well as by K_3, K_4, and K_5. A small K_2/K_1 ratio corresponds to weak coupling as well as small dispersion for both the ν_1 and ν_2 branches while increasing the Pt-Pt interaction K_5, for example, has little effect on the zone center ν_2 phonon since all the Pt atoms move in phase, but increases the frequency of the zone boundary ν_2 phonon where Pt atoms in adjacent cells move in opposite directions, thus decreasing the normally downward dispersion of this branch.

The simulated spectra in Fig. 8 are presented, from top to bottom, in order of decreasing dispersion of the ν_2 branch. In Fig. 8(a), the K_2/K_1 ratio is 2/3 ($K_1=132.7$, $K_2=88.5$ N/m, $K_3=K_4=K_5=0$) resulting in strong coupling between neighboring cells and a dispersion of 7.3 cm^{-1} downward from zone center to zone boundary. In Fig. 8(b), we use $K_1=166$, $K_2=45.4$ N/m, $K_3=K_4=-4.7$ N/m, and $K_5=0$. The coupling is considerably smaller, K_2/K_1 being 0.27, but the dispersion is only slightly less, 6.8 cm^{-1}; the large dispersion here arises from the large negative values of K_3 and K_4. In Fig. 8(c), we keep $K_1=166$, $K_2=45.4$ N/m, and $K_5=0$,

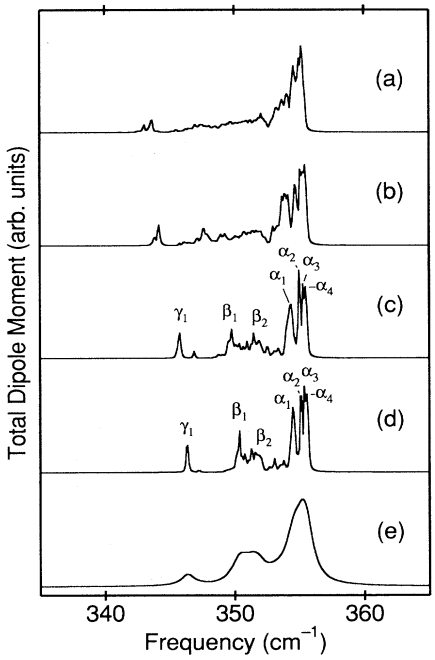

FIG. 8. Simulated infrared absorption spectra in the ν_2 region for a Pt-Cl chain with randomly distributed Cl isotopes in their natural abundance, showing the effect of choice of spring constants, and, in particular, the effect of the dispersion of the ν_2 branch. The spring constants and dispersion are as follows: (a) $K_1=132.7$, $K_2=88.5$ N/m, $K_3=K_4=K_5=0$, dispersion=7.3 cm^{-1}; (b) $K_1=166$, $K_2=45.4$, $K_3=K_4=-4.7$ N/m, $K_5=0$, dispersion=6.8 cm^{-1}; (c) $K_1=166$, $K_2=45.4$, $K_3=K_4=-2.3$ N/m, $K_5=0$, dispersion=4.1 cm^{-1}; (d) $K_1=166$, $K_2=45.4$, $K_3=K_4=-2.3$, $K_5=36$ N/m, dispersion=3.4 cm^{-1}. In (a)–(d) the phenomenological linewidth is set to 0.1 cm^{-1}. In (e) the same simulated spectrum as in (d) is shown, but with the phenomenological linewidth set to 1.2 cm^{-1}. Eigenvectors for the peaks labeled α_1 through γ_2 in (c) and (d) are shown in Fig. 9.

but set $K_3 = K_4 = -2.3$ N/m, reducing the dispersion to 4.1 cm^{-1}. Finally, in Fig. 8(d), we maintain the first four constants at $K_1 = 166$, $K_2 = 45.4$, $K_3 = K_4 = -2.3$ N/m, but now set $K_5 = 36$ N/m. This is the set of force constants we had previously used to reproduce the observed fine structure for both the ν_1 and ν_2 branches.

In each of these first four simulated spectra, the width (full width at half maximum) of the Lorentzian line shapes assigned to each normal mode is fixed at 0.1 cm^{-1}, this rather small value making it possible to see in detail the complex fine structure arising from the randomly distributed ^{35}Cl and ^{37}Cl isotopes. We emphasize that all the peaks seen in these simulations are reproducible and physically meaningful, and are not, for example, simply artifacts of the finite number of atoms used in the simulations. As was first realized by Dean,[31,32] who performed similar calculations on random two-component chains consisting of tens of thousands of atoms, such structure never smooths out with increasing number of atoms.[33–35] Each peak in Fig. 8 corresponds to a *localized* normal mode of the chain, associated with a specific sequence of ^{35}Cl and ^{37}Cl isotopes. The strength of a given peak is determined by a combination of the probability of occurrence for that particular isotope sequence and the dipole moment of the associated localized mode.

The trend we see in Figs. 8(a)–8(d) is that for the large dispersion, strong-coupling regime of Fig. 8(a), the number of localized modes is very large and they are spread out into a broad quasicontinuous band. As the dispersion of the ν_2 branch is decreased, the modes gradually become more and more clumped around a few distinct frequencies, eventually approaching the three-peaked structure observed experimentally.

By the time the dispersion has been reduced to the degree shown in Fig. 8(c), the number of prominent peaks in the spectrum is small enough that the eigenvectors and the particular sequences of Cl isotopes responsible for each peak can be easily examined. In Figs. 8(c) and 8(d) we have labeled the most prominent peaks α_1, α_2, α_3, α_4, β_1, β_2, and γ_1. Figure 9 shows the isotopic sequences and atomic displacement eigenvectors for the normal modes giving rise to each of these peaks.

Qualitative insight into the nature of these modes can be gained by noting that, because the vibrational amplitude for each mode is concentrated on just a few unit cells, the character of a mode centered on a given Cl-Pt-Cl unit is determined almost entirely by the Cl isotopes on the nearest- and next-nearest-neighbor units surrounding it. Thus, to a good approximation, these modes act as if they were localized on isolated defects in an infinite chain of a type defined by the immediate neighborhood of the center unit. Thus, the peak labeled α_1 arises from a single 35-35 unit surrounded on either side by 35-37 units. The normal mode associated with this sequence can be approximated quite well by the local mode for 35-35 defect in an infinite 35-37 chain. Likewise the β_1 and γ_1 peaks correspond, respectively, to a single 35-37 unit surrounded by 35-35 units and to a single 37-37 unit surrounded by 35-35*s*; the two associated localized modes can be approximated by the gap modes for isolated 35-37 or 37-37 defects, respectively, in a 35-35 chain.

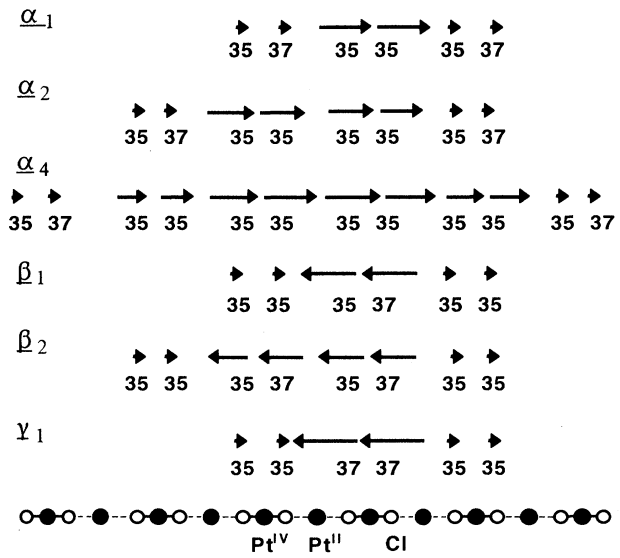

FIG. 9. Eigenvectors for the most frequently occurring and most strongly IR-active localized vibrational modes of a PtCl chain with randomly distributed ^{35}Cl and ^{37}Cl isotopes. Shown here are the Cl isotope sequences and Cl displacements for the normal modes associated with the six strongest peaks in the simulated spectra in Figs. 8(c) and 8(d). Eigenvector labels α_1 through γ_1 correspond to the peak labels in Fig. 8. Pt displacements, omitted for clarity, are opposite the Cl displacements within a given unit cell.

The cluster of peaks labeled β_2 corresponds to pairs of 35-37 units surrounded by 35-35*s* and the vibrational modes responsible are again of gap mode character. The ordering of the isotopes within the 35-37 units has only a small effect on the frequency of these modes; the various peaks clustered in the β_2 region arise from the various permutations of isotope ordering.

Finally, the sequence of peaks α_2, α_3, α_4, corresponds to successively longer segments of pure ^{35}Cl chain; the α_2 peak corresponds to a pair of 35-35 units terminated on either end by 35-37 or 37-37 units, while the α_3 and α_4 peaks correspond, respectively, to three and four consecutive 35-35 units. Figure 9 shows the eigenvectors for the two- and four-unit segments. All of these modes are similar in character to nonzero wave-vector ν_2 phonons, with the shorter segments corresponding to the larger wave vectors. Thus, the ordering of these peaks—higher frequency for longer segments—makes qualitative sense given that this phonon branch disperses downward with increasing wave vector.

As the spring constants are adjusted so as to increase the coupling between Cl-Pt-Cl units and also increase the dispersion of the ν_2 phonon branch, as in Figs. 8(a) and 8(b), the eigenvectors become less highly localized, with the vibrational amplitude for a given mode spread over a longer sequence of isotopes. Thus, many more distinct kinds of modes are possible, and the resulting spectra show a multitude of peaks. The larger dispersion, moreover, spreads the various modes over a larger frequency

region. When the coupling and dispersion are reduced, on the other hand, as in Fig. 8(d), the frequencies of all modes localized on 35-35 segments (i.e., those labeled α) approach a single value. The same is true for the 35-37 modes (β) and the much rarer 37-37 modes (γ).

The key, then, to making the ν_2 fine structure collapse into the observed three peaks, is to require the dispersion of the ν_2 branch to be small. As can be seen in Fig. 8(e), which shows the same simulated spectrum as in Fig. 8(d), but with the phenomenological line width increased to 1.2 cm^{-1}, this last set of spring constants, yielding a ν_2 branch dispersion of 3.4 cm^{-1}, already does quite a good job of reproducing the observed structure. The slightly double-peaked appearance of the central peak would probably be just observable experimentally, so we suggest that an upper limit on the magnitude of the actual dispersion for the ν_2 branch is around 3 cm^{-1}.

Comparing these results with our earlier simulations on the Raman-active ν_1 phonon reveals that the apparent discrepancy between the fine structures of these two modes is mainly a matter of the ordering and spacing of the various local modes, and that, in fact, the fundamental mechanism leading to the fine structure—vibrational localization on "islands" defined by a few highly probable sequences of isotopes—is the same in both cases. Indeed, comparing Fig. 9 with the corresponding Raman eigenvectors in Ref. 30, one finds that the isotopic sequences are the same for the Raman and IR features. The 315.4-, 313.4-, 309.0-, 308.2-, and 305.4-cm^{-1} Raman modes seen in Fig. 7(a) result from modes localized on the same kind of segments as those responsible, respectively, for the features α_1, α_2, β_1, β_2, and γ_1 in the IR simulation, while the 312.0 cm^{-1} Raman feature corresponds to α_3 and α_4. The fundamental differences between the two cases are the magnitude and direction of the dispersion of the two phonon branches.

The problem is how to choose the set of force constants so as to obtain small dispersion in ν_2 and still get the $\sim$6.5-cm^{-1} dispersion in the ν_1 branch necessary to reproduce the Raman fine structure. The only way to do so in this model is to allow the Pt-Pt interaction, K_5, to assume a large value, comparable to that of K_2. As already mentioned, increasing K_5 raises the frequency of the zone boundary ν_2 phonon because here the Pt atoms in adjacent cells move out of phase, while only slightly affecting the zone center ν_2 mode, and not affecting the ν_1 branch at all since the ν_1 modes involve no Pt motion. A value of 36 N/m for K_5, we have seen, does a fair job of reproducing the observed features, but larger values of around 50 N/m do even better. It is interesting to note that here we have a case whereby increasing the coupling between Cl-$Pt^{III+\delta}$-Cl units, by increasing K_5, we create a situation which mimics the case of no coupling at all. The latter has zero dispersion for any of the phonons, and, of course, is just the case of isolated $PtCl_2$ molecules; so it is clear that for this case there must be only three components to the Cl isotopic structure. But what is remarkable is that another set of spring constants, which produces small dispersion for completely different reasons, will, in fact, produce the same spectroscopic result.

The question is whether such a large value of K_5 is physically reasonable. We find that because the Pt ions are highly charged—Pt^{3+} for the case of no CDW or Pt^{2+} and Pt^{4+} for the strong CDW case—the Coulomb repulsion between these ions, if unscreened, could, in principle, lead to values for K_5 which are comparable to K_1 and K_2. To estimate the magnitude of K_5 arising just from the Coulomb repulsion of the Pt ions, consider the following one-dimensional case. Let three colinear point charges, all positive, of magnitudes q_1, q_2, and q_1, in that order, corresponding to three consecutive Pt ions on the chain, be constrained to move along the line connecting them. Let the equilibrium distance between the charges be denoted d. Holding the positions of the outer two ions fixed and displacing the center ion by a distance δx, the center ion experiences a restoring force $F(\delta x)$ given by

$$F(\delta x)=\frac{q_1 q_2}{4\pi\varepsilon_0}\left[\frac{1}{(d+\delta x)^2}-\frac{1}{(d-\delta x)^2}\right], \tag{1}$$

which, in the limit of infinitesimal δx, reduces to

$$\lim_{\delta x\to 0} F(\delta x)=-\left[\frac{1}{4\pi\varepsilon_0}\right]\left[\frac{4q_1 q_2}{d^3}\right]\delta x\equiv -2K_5\delta x\ . \tag{2}$$

For the totally unscreened case, for which ε_0 is the permittivity of free space, setting $q_1=+4$ and $q_2=+2$ electron charges, and setting the equilibrium distance d equal to the known $Pt^{III-\delta}$—$Pt^{III+\delta}$ spacing[24,26] of 5.4 Å for PtCl, Eq. (2) yields a K_5 value of 23 N/m.

Coulomb repulsion, however, is not the only effect contributing to K_5. Recent work on the structural, electronic, and vibrational effects of varying the species forming the hydrogen-bonded ligand-counterion bridge between the metals shows that the stiffness of this bridge, compared to that of the chain, is quite substantial,[42,43] and that the choice of the ligand-counterion bridge is the dominant factor determining the Pt-Pt separation. Thus, large K_5 values seem quite likely. This affects not only the dispersion of the ν_2 phonon branch, but also strongly affects the frequency of the ν_3 phonon, which is essentially at Pt-Pt stretch. If a large Pt-Pt interaction exists for PtCl, it also probably exists for PtBr and PtI. As we shall see, this has important implications for identifying the chain phonons, particularly ν_3, in all these materials.

3. *PtCl ν_3*

Identification of the low-frequency IR chain phonon, ν_3, in PtCl is considerably more ambiguous than was the case for ν_2. The authors of Ref. 21 assign the feature near 145 cm^{-1} (our mode G) to the ν_3 mode (those authors put the frequency at 137 cm^{-1}, a discrepancy probably arising in their Kramers-Kronig analysis versus our transmittance measurements). This assignment seems dubious in view of the substantial evidence in the present data indicating that this is a ligand mode, i.e., its large shift upon deuteration and its presence in both PtBr and PtI. Moreover, our model predicts a dipole moment for

ν_3 in PtCl which is roughly 2 orders of magnitude smaller than that of ν_2. This is because ν_3 involves motion primarily of the heavy Pt ions, and thus has smaller amplitude, and also because the motion of the negatively charged Cl^- ions in the ν_3 mode tends to cancel the dipole moment associated with the Pt ion motion (see Fig. 2). Thus, it seems unlikely that ν_3 should appear as an IR feature of strength comparable to that of ν_2.

In our spectra we do note a feature at 167.3 cm^{-1} which displays a Cl isotope fine structure similar to that of the ν_2 mode. In Fig. 10, which shows this frequency region for (a) the natural Cl isotopic abundance sample and (b) the highly enriched $Pt^{35}Cl$ sample, three absorption peaks, at 167.3, 165.6, and 163.4 cm^{-1}, can be seen in the natural abundance sample, while only the strong 167.3-cm^{-1} peak remains in the isotopically pure $Pt^{35}Cl$ sample. This clearly demonstrates that this mode is associated with the Pt-Cl chains and involves substantial Cl motion.

Determining whether this feature is the ν_3 mode or something else, perhaps a bending mode, requires an examination of its polarization, frequency, and the isotopic fine structure. Unfortunately, the polarization of this feature is uncertain because in this region of the chain-polarized reflectivity data of Ref. 21, all features merge into a single broad band, extending tens of cm^{-1}, which may or may not include a contribution from this mode.

The frequency of 167.3 cm^{-1} at first seems rather high for the ν_3 mode, based on the simplest lattice-dynamics model with only the nearest-neighbor harmonic interactions K_1 and K_2; for this case, given that $\nu_1=311$ cm^{-1} and $\nu_2=355.8$ cm^{-1}, one predicts ν_3 to be at 69.6 cm^{-1}. But this simplest case, for which $K_1=183.9$ N/m and $K_2=17.0$ N/m, fails to produce dispersion in the ν_1 branch sufficient to account for the observed Raman isotopic fine structure. As discussed in the preceding section, in order to simultaneously reproduce the ν_1 and ν_2 fine structure, the model must have more nearly equal K_1 and K_2 to produce the required dispersion in the ν_1 branch, and at the same time include a large $Pt^{III-\delta}$—$Pt^{III+\delta}$ interaction, K_5, to reduce the dispersion of the ν_2 branch in order to reproduce the observed IR fine structure. A large $Pt^{III-\delta}$—$Pt^{III+\delta}$ force constant, however, also has the effect of driving up the frequency of the ν_3 mode, since this mode is primarily a $Pt^{III-\delta}$—$Pt^{III+\delta}$ stretch.

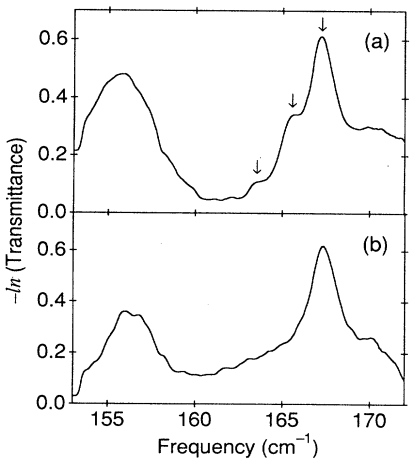

FIG. 10. Far-infrared spectra of PtCl showing the fine structure on the 167.3 cm^{-1} feature. (a) PtCl with natural Cl isotopic abundance. (b) PtCl with ~99% ^{35}Cl. Note the three peaks marked with arrows in (a), in contact to the single 167.3-cm^{-1} peak seen in (b).

When the value $K_5=23$ N/m, as calculated from the Coulomb repulsion of the Pt ions in the preceding section, is used in the model while keeping the other force constants the same as for Figs. 7(d) and 7(e), a frequency of 138 cm^{-1} is predicted for the zone center ν_3 phonon in the pure $Pt^{35}Cl$ chain. With the likely additional contribution to K_5 from the ligand-counterion-ligand bridge discussed above, a ν_3 frequency of 167 cm^{-1} appears not out of the question.

But the model also predicts a very large dispersion for the ν_3 branch, with the zone boundary frequency falling at 99 cm^{-1} for the case with $K_5=23$ N/m; hence, the localized modes for isolated heavy isotopes must fall below 99 cm^{-1}. More importantly, however, the large dispersion is correlated with strong effective coupling between cells for this mode, with the result that vibrational amplitude is *not* strongly localized for this case, implying that no isotopic fine structure would be observed for ν_3. The simulated spectrum for the ν_3 region bears this out, and displays only a single peak at 138 cm^{-1} with no fine structure. The observed structure, in contrast, with its three peaks spaced by only about 2 cm^{-1}, implies that the phonon responsible for the 167.3 cm^{-1} peak has virtually no dispersion.

Because the harmonic model is admittedly a rather crude approximation for these materials, despite its success in describing the ν_1 and ν_2 branches, this dispersion problem may not definitively rule out the assignment of the 167.3-cm^{-1} feature to the ν_3 phonon. It does, however, cast serious doubt, and we currently favor the assignment of this feature to the bending mode of the Cl-$Pt^{III+\delta}$-Cl units, with motion transverse to the chain. Definitive resolution of this question will have to await further experiments, in particular, the determination of the polarization of the 167.3-cm^{-1} feature.

4. *PtBr ν_2*

Applying this same harmonic model to PtBr chains, starting with the known frequency of 165 cm^{-1} for the Raman-active ν_1 mode,[22] one predicts a ν_2 frequency somewhere above 200 cm^{-1} for any physically reasonable set of spring constants. The only feature falling in this frequency region of the FIR spectrum of PtBr is the strong mode at 238.7 cm^{-1}.

Several other arguments favor assigning the 238.7-cm^{-1} feature of PtBr to the ν_2 chain phonon: (1) It is unique to PtBr; no corresponding feature is apparent in either PtCl or PtI. (2) This feature is chain polarized, as

demonstrated in Ref. 21. (3) This mode shows very little frequency shift upon deuteration. The small shift which does occur appears to be largely the result of coupling to mode E as it shifts down from above and collides with the 238.7-cm^{-1} mode. So in this case, the best estimate for the isolated chain value of ν_2 comes from the undeuterated samples, unlike in PtCl where coupling to ligand modes was least important for the completely deuterated case.

Thus, the present results support the assignment of this feature to the ν_2 mode by Ref. 21. [We note a sizable discrepancy between our frequency of 238.7 cm^{-1} and the value of 28 meV (226 cm^{-1}) reported in the text and tables of Ref. 21. Direct examination of the data presented in Ref. 21, however, suggests that the 28 meV value is not consistent with their reflectivity spectrum, and is perhaps the result of an error. Judging from the shape and position of the reflectivity peak shown in Ref. 21, our best estimate for the TO frequency is 29.5 meV (238 cm^{-1}), in excellent agreement with our results. Given the extreme sharpness of the reflectivity peak, such a direct intuitive extraction of the TO frequency from the reflectivity spectrum is probably quite accurate.]

It should be noted that, for PtBr, the harmonic linear chain model is not nearly as satisfying as it was for the PtCl case. Given that $\nu_1=165$ cm^{-1} and $\nu_2=238.7$ cm^{-1}, a good fit to the experimental results is obtained with $K_1=136.5$, $K_2=38$, $K_3=K_4=-11.3$, $K_5=36$ N/m. The large negative values of K_3 and K_4, however, do not seem physically reasonable (small negative values might be rationalized by arguing that, since the force constants are not independent, that this is merely a roundabout way of including anharmonicity and asymmetry of the potentials in this harmonic treatment). But without using negative K_3 and K_4, it is not possible to find a set of spring constants such that the model yields a ν_2 frequency as high as the observed frequency of 238.7 cm^{-1}. If, for instance, we use the Coulomb repulsion value of 23 N/m for the Pt-Pt force constant, K_5, set the ration $K_2/K_1=1/2$, and keep $K_3=K_4=0$, the model predicts zone center values $\nu_2=201$ cm^{-1} and $\nu_3=129$ cm^{-1}. Decreasing the ratio K_2/K_1 in general increases ν_2 while decreasing ν_3. Thus, keeping the same value of K_5, we obtain $\nu_2=211$ cm^{-1} and $\nu_3=114$ cm^{-1} for $K_2/K_1=1/4$; $\nu_2=219$ cm^{-1} and $\nu_3=97$ cm^{-1} for $K_2/K_1=1/9$; and finally, $\nu_2=227$ cm^{-1} and $\nu_3=76$ cm^{-1} for $K_2=0$.

This appears to indicate that K_2/K_1 is small in PtBr, but all other indications are to the contrary: Structural studies reveal a smaller Peierls distortion than in PtCl, which, in turn, implies a weaker CDW and more nearly equal K_1 and K_2. The lack of any observable Br isotopic fine structure in either the FIR or Raman spectra implies further that this system is in the strongly coupled regime (i.e., large K_2/K_1) for which the vibrational modes are delocalized. Thus, it appears that this model is too oversimplified for this material; a more complete model which includes anharmonicities and long-range interactions, perhaps involving the ligands and counterions, is apparently necessary in order to fit the observed behavior.

5. *PtBr ν_3*

The large number of features in the low-frequency region of the PtBr spectra, both in this work and in Ref. 21, together with the extreme sensitivity of the ν_3 frequency to small changes in spring constants in the lattice-dynamics models, makes assignment of any given spectral feature to the ν_3 phonon virtually impossible without further experiments (e.g., single-crystal uniaxial stress measurements). The authors of Ref. 21 put the ν_3 frequency at 96.8 cm^{-1}, but we find little justification for this assignment. Positive identification of the ν_3 mode in PtBr will have to await more extensive experimental studies, and may be extremely difficult, given the expected small dipole moment for ν_3.

6. *PtI ν_2 and ν_3*

PtI displays three strong features, at 184.2, 129.7, and 87.3 cm^{-1}, unique to this material, two of which most likely arise from the ν_2 and ν_3 modes. We find that the 184.2- and 87.3- cm^{-1} features undergo virtually no shift upon deuteration of the ligands, while the small shift of the 129.7-cm^{-1} feature can be attributed to coupling to the strongly shifting mode G. The results of Ref. 21 show that all three of these modes are chain polarized.

Applying the harmonic linear chain model to PtI, using the best available ν_1 frequency of 112 cm^{-1} obtained from our recent Raman studies, reasonable values for spring constants always put the ν_2 frequency somewhere above 140 cm^{-1}, making the observed 184.2 cm^{-1} feature the best candidate for ν_2. But the model fails in the same manner as it did for PtBr—no physically reasonable set of spring constants can yield a ν_2 value as high as 184.2 cm^{-1} while keeping ν_1 at 112 cm^{-1}.

We note that, because of the greater mass of the I^- ion and the smaller charge disproportionation on the Pt ions (weaker CDW), PtI, unlike PtCl and PtBr, should have a ν_3 dipole moment on the same order of magnitude as that of ν_2, thus making it likely that ν_3 can be observed. Which of the two remaining observed features, if either, corresponds to the ν_3 phonon is problematical. The initial prejudice was that ν_3 should always be less than ν_1, thus making the 87.3-cm^{-1} feature the best candidate, as was suggested in Ref. 21. But this assumption has been based on models which neglect the possibility of a large Pt-Pt interaction due to Coulomb repulsion between these highly charged ions. If we use our calculated value $K_5=23$ N/m, along with the physically reasonable ratio $K_2/K_1=1/2$, the model predicts $\nu_1=112$ cm^{-1}, $\nu_2=153$ cm^{-1}, and $\nu_3=116$ cm^{-1} for the zone center phonons (note that ν_3 is now higher than ν_1), making the 129.7-cm^{-1} feature a reasonable candidate for the ν_3 mode. The even stiffer K_5 value suggested by the ligand-counterion-ligand bridge discussed above adds further weight to this latter assignment. Further experiments and more refined modeling will be required to resolve this question.

IV. SUMMARY AND CONCLUSIONS

The isotopic substitution studies described here have enabled us to resolve several important ambiguities in the assignments of infrared-active modes in the *MX* materials, as well as to uncover some important fundamental physics. For the case of PtCl, the observation of Cl isotopic fine structure, the isotopic origin of which is confirmed by examination of a nearly pure $Pt^{35}Cl$ sample, has permitted us to conclusively identify the ν_2 asymmetric stretch chain mode. Questions about the details of this fine structure, and why it differs radically from that associated with the Raman-active ν_1 symmetric stretch chain mode, led to lattice-dynamics simulations on a harmonic-linear-chain model with randomly distributed ^{35}Cl and ^{37}Cl isotopes. The results of these simulations show that the origin of the fine structure in both the ν_1 and ν_2 branches is the result of a breakdown of the extended phonon picture due to the disorder of the Cl isotopes; the observed fine structure arises from highly localized vibrational modes residing on a few distinct sequences of ^{35}Cl and ^{37}Cl isotopes which occur with high probability. These results, along with our recent Raman results,[30] provide the first direct experimental confirmation of long-standing predictions on the behavior of disordered one-dimensional chains.

The surprising discrepancy between the ν_1 and ν_2 fine structures turns out to be the result of quite minor differences in the dispersions of the two phonon branches. Fitting the observed isotopic fine structure in this manner enables us to indirectly determine the dispersion for these two phonon branches: in order to obtain the observed three-peaked structure, the dispersion of the ν_2 phonon branch in the pure ^{35}Cl material must be downward from Brillouin zone center boundary and of magnitude less than 3 cm^{-1}, whereas our earlier work showed that the ν_1 dispersion must be upward by about 6.5 cm^{-1}. Thus, the effects of disorder can be utilized to provide a novel method of determining phonon dispersions by purely optical means, a technique which should be applicable to many other 1D systems.

A final important result of this analysis is that the small value for the ν_2 dispersion could only be obtained in the modeling by setting the Pt-Pt force constant to a large value. This is consistent with unscreened Coulomb repulsion between these highly charged ions. The implication is that Pt-Pt interactions play an important role in the vibrational properties of all these materials.

The observation of a similar three-peaked fine structure for the feature at 167.3 cm^{-1}, which again is confirmed to be the result of Cl isotopes by the absence of such structure in the enriched $Pt^{35}Cl$ material, show that this feature also arises from a chain mode. The frequency of this feature is much higher than initially anticipated for the ν_3 mode, but when the Coulomb repulsion between Pt ions is considered, a ν_3 frequency this high does not appear physically unreasonable. The more important argument against this assignment, however, is that the dispersion of the ν_3 branch should be very large, which should result in a washing out of any isotopic fine structure. A more satisfying assignment for this feature would be a chain bending mode, with Cl motion perpendicular to the chain axis.

In all three materials, we have identified several features which, because of their large frequency shifts upon ligand deuteration, must be attributed to modes primarily involving motion of the ethylenediamine ligands. This permits these features to be eliminated from consideration as possible candidates for chain modes. Furthermore, these observations demonstrate that two earlier assignments in Ref. 21 are clearly incorrect: Those authors' assignment of the $\sim$266-cm^{-1} feature (our mode *E*), appearing in all three Pt*X* materials, to a localized chain bending mode associated with polaron defects, and their assignment of the $\sim$145-cm^{-1} feature (our mode *G*) in PtBr to a localized gap mode of the polaron defect are both refuted by the large deuteration shifts of these features, as well as by their halogen independence and by their extreme strength (comparable to or greater than that of the fundamental ν_2 reststrahl).

In PtBr, the strong feature at 238.7 cm^{-1} can be assigned with a reasonable degree of confidence to the ν_2 phonon, since this feature is unique to PtBr, displays little shift upon ligand deuteration apart from that attributable to coupling to a nearby ligand mode, lies in the right frequency region, and was shown in Ref. 21 to be chain polarized. Similar arguments favor the assignment of the 184.2-cm^{-1} feature in PtI to the ν_2 phonon of that material.

We are unable, however, to identify the ν_3 mode in PtBr. The complexity of the low-frequency region of the spectrum of this material, coupled with the extreme sensitivity of ν_3 to the choice of force constants in lattice-dynamics modeling, leaves no clear choice for the PtBr ν_3 mode. Because of these difficulties, we also find no justification for the assignment suggested in Ref. 21.

Two features in PtI may be considered candidates for the ν_3 mode of that material. The first, at 87.3 cm^{-1}, is the best choice if Pt-Pt interactions are assumed to be small, i.e., if substantial screening of the ionic charges occurs, while the second, at 129.7 cm^{-1}, provides the best agreement to the case of unscreened Pt-Pt interactions and a stiff ligand-counter-ion bridge. The present data cannot definitively distinguish between these alternatives.

An important result of the ethylenediamine ligand deuteration experiments is that, for all these materials, the chain modes are observed to shift somewhat as the ligand modes are shifted by deuteration, and are perturbed substantially when the ligand and chain modes become close in frequency. The implication is that the ligand modes couple to and mix with the Pt*X* chain modes, so that, in general, the observed features actually correspond to modes involving both chain and ligand motion. This effect is not surprising, but the size of the perturbation raises questions about the extent to which the approximation of isolated *MX* chains can be used to model these materials. While qualitative effects may be predicted quite well in the isolated chain approximation, any theory which hopes to accurately describe the vibrational behavior of these materials cannot ignore the effects of the ligands and counterions, but must consider the entire

structure.

Finally, we note that the isotopic fine structure observed in both the IR and Raman spectra of PtCl, and the general principle reinforced by these observations—that vibrational modes localized on finite chain segments can have substantially different frequencies from those of the zone center phonons of an infinite chain—has important implications for understanding the spectra of other MX materials. The strong excitation energy dependence and multiple peaks seen for the Raman spectrum in the ν_1 region of PtBr, for instance, could very well have their origin in finite chain segments demarcated not by isotopes, but by photoinduced defects. A reexamination of several of the puzzling features of MX chain spectra, bearing in mind these ideas, might well resolve some long-standing questions.

ACKNOWLEDGMENTS

The authors would like to thank R. J. Donohoe, A. D. F. Bulou, L. H. Jones, and A. R. Bishop for enlightening discussions. This work was supported by the Materials Science Division of the U.S. Department of Energy Office of Basic Energy Sciences, and by the Center for Materials Science at Los Alamos National Laboratory.

APPENDIX: DETAILS OF THE 1D LATTICE-DYNAMICS CALCULATIONS

For the 1D lattice-dynamics modeling used here for qualitative insight in making assignment and for understanding the isotopic fine structure in PtCl, we use the standard formalism as outlined by Barker and Sievers.[35] For a 1D chain with harmonic springs as illustrated in Fig. 2, the equations of motion, assuming simple harmonic solutions of frequency ω, can be written in matrix form as

$$-\omega^2 \underline{M}\mathbf{x} = -\underline{k}\mathbf{x} , \tag{A1}$$

where the atomic displacements are contained in the column vector $\mathbf{x}$, $\underline{M}$ is a diagonal matrix with nonzero elements M_{ii} equal to the mass of the ith atom, and $\underline{k}$ is the spring constant matrix, defined below for the model shown in Fig. 2. In constructing the matrices, we use the ordering convention of letting M_{11} correspond to the halogen atom to the left of $Pt^{III+\delta}$, M_{22} to $Pt^{III+\delta}$, M_{33} to the halogen atom to the right of $Pt^{III+\delta}$, M_{44} to $Pt^{III-\delta}$, and so on. With this convention, the nonzero elements of the spring constant matrix $\underline{k}$ for the model shown in Fig. 2 are

$$\begin{aligned}
&k_{11} = (K_1 + K_2 + K_3 + K_4) , \\
&k_{22} = (2K_1 + 2K_5) , \\
&k_{33} = (K_1 + K_2 + K_3 + K_4) , \\
&k_{44} = (2K_2 + 2K_5) , \\
&k_{12} = k_{21} = k_{23} = k_{32} = -K_1 , \\
&k_{34} = k_{43} = k_{45} = k_{54} = -K_2 , \\
&k_{13} = k_{31} = -K_3 , \\
&k_{24} = k_{42} = -K_5 , \\
&k_{35} = k_{53} = -K_4 , \\
&k_{46} = k_{64} = -K_5 .
\end{aligned} \tag{A2}$$

For an arbitrarily long chain, these elements repeat according to the recursion relation

$$k_{4n+i,4n+j} = k_{ij} \quad (n = 1,2,3,\ldots) . \tag{A3}$$

Finally, the use of periodic boundary conditions, for a chain of length N (equal to four times the number of unit cells), leads to elements in the upper right and lower left corners of the matrix:

$$\begin{aligned}
&k_{1,N} = k_{N,1} = -K_2 , \\
&k_{1,N-1} = k_{N-1,1} = -K_4 , \\
&k_{2,N} = k_{N,2} = -K_5 .
\end{aligned} \tag{A4}$$

Defining the diagonal matrices $\underline{M}^{\pm 1/2}$ by

$$(\underline{M}^{\pm 1/2})_{ii} \equiv (\underline{M}_{ii})^{\pm 1/2} , \tag{A5}$$

and the normalized displacements

$$\mathbf{u} \equiv \underline{M}^{+1/2}\mathbf{x} , \tag{A6}$$

Eq. (A1) reduces to the diagonalization problem

$$(\underline{D} - \omega^2 \underline{I})\mathbf{u} = \mathbf{0} , \tag{A7}$$

where the dynamical matrix $\underline{D}$ is defined by

$$\underline{D} \equiv \underline{M}^{-1/2}\underline{k}\,\underline{M}^{-1/2} . \tag{A8}$$

This matrix is diagonalized using standard computer routines to obtain the frequency eigenvalues and displacement eigenvectors.

Solving the diagonalization problem for a two-unit-cell (eight-atom) chain gives the zone center and zone boundary phonons, which is sufficient for the purposes of exploring the effects of various force constants and for estimating relative sizes of the electric dipole moments for different modes. For the Cl-isotopic fine-structure calculations, 32-unit-cell (128-atom) chains, with the appropriate random distributions of Cl isotopes, are used, and the results for 100 such chains combined to obtain the simulated IR and Raman spectra.

[1]D. Baeriswyl and A. R. Bishop, Phys. Scr. **T19**, 239 (1987).
[2]D. Baeriswyl and A. R. Bishop, J. Phys. C **21**, 339 (1988).
[3]A. Mishima and K. Nasu, Phys. Rev. B **39**, 5758 (1989).
[4]S. D. Conradson, M. A. Stroud, M. H. Zietlow, B. I. Swanson, D. Baeriswyl, and A. R. Bishop, Solid State Commun. **65**, 723 (1988).
[5]J. T. Gammel, R. J. Donohoe, A. R. Bishop, and B. I. Swanson, Phys. Rev. B **42**, 10 566 (1990).
[6]R. J. Donohoe, C. D. Tait, and B. I. Swanson, Chem. Mater. **2**, 315 (1990).
[7]R. J. Donohoe, S. P. Love, M. A. Y. Garcia, and B. I. Swanson, in *Frontiers of High Pressure Research,* edited by H. D. Hochheimer and R. D. Etters, NATO ASI Series B: Physics, Vol. 286 (Plenum, New York, 1991), pp. 73–85.
[8]L. V. Interrante, K. W. Browall, and F. P. Bundy, Inorg. Chem. **13**, 1158 (1974).
[9]N. Kuroda, M. Sakai, Y. Nishina, M. Tanaka, and S. Kurita, Phys. Rev. Lett. **58**, 2122 (1987).
[10]H. Tanino, N. Koshizuka, K. Kobayashi, M. Yamashita, and K. Hoh, J. Phys. Soc. Jpn. **54**, 483 (1985).
[11]B. I. Swanson, M. A. Stroud, S. D. Conradson, and M. H. Zietlow, Solid State Commun. **65**, 1405 (1988).
[12]K. Toriumi, Y. Wada, T. Mitani, S. Bandow, M. Yamashita, and Y. Fujii, J. Am. Chem. Soc. **111**, 2341 (1989).
[13]R. J. Donohoe, S. A. Ekberg, C. D. Tait, and B. I. Swanson, Solid State Commun. **71**, 49 (1989).
[14]R. J. Donohoe, R. B. Dyer, and B. I. Swanson, Solid State Commun. **73**, 521 (1990).
[15]K. Nasu, J. Phys. Soc. Jpn. **52**, 3865 (1983); **53**, 302 (1984); **53**, 427 (1984); **54**, 1933 (1985); Phys. Rev. B **44**, 7625 (1991).
[16]A. Mishima and K. Nasu, Synth. Met. **29**, F175 (1989).
[17]K. Iwano and K. Nasu, J. Phys. Soc. Jpn. **61**, 1380 (1992).
[18]J. T. Gammel, A. Saxena, I. Batistic, and A. R. Bishop, Phys. Rev. B **45**, 6408 (1992); S. M. Weber-Milbrodt, J. T. Gammel, A. R. Bishop, and E. Y. Loh, *ibid.* **45**, 6435 (1992).
[19]X. Z. Huang, A. Saxena, A. R. Bishop, L. A. Worl, S. P. Love, and B. I. Swanson, Solid State Commun. **84**, 957 (1992).
[20]A. D. F. Bulou, R. J. Donohoe, and B. I. Swanson, J. Phys.: Condens. Matter **3**, 1709 (1991).
[21]L. Degiorgi, P. Wachter, M. Haruki, and S. Kurita, Phys. Rev. B **42**, 4341 (1990).
[22]S. C. Huckett, R. J. Donohoe, L. A. Worl, A. D. F. Bulou, C. J. Burns, J. R. Laia, D. Carroll, and B. I. Swanson, Chem. Mater. **3**, 123 (1991).
[23]H. J. Keller, B. Müller, G. Ledezma, and R. Martin, Acta Crystallogr. C **41**, 16 (1985).
[24]N. Matsumoto, M. Yamashita, I. Ueda, and S. Kida, Mem. Fac. Sci., Kyushu University, Ser. C **11**, 209 (1978).
[25]J. B. Weinrach, S. A. Ekberg, S. D. Conradson, and B. I. Swanson, Inorg. Chem. **29**, 981 (1990).
[26]S. C. Huckett, B. Scott, S. P. Love, R. J. Donohoe, C. J. Burns, E. Garcia, T. M. Frankcom, and B. I. Swanson, Inorg. Chem. (to be published).
[27]K. Toriumi, M. Yamashita, S. Kurita, I. Murase, and T. Ito, Acta Crystallogr. B (to be published).
[28]L. Degiorgi, P. Wachter, M. Haruki, and S. Kurita, Phys. Rev. B **40**, 3285 (1989).
[29]S. D. Allen, R. J. H. Clark, V. B. Croud, and M. Kurmoo, Philos. Trans. R. Soc. London, Ser. A **314**, 131 (1985).
[30]S. P. Love, L. A. Worl, R. J. Donohoe, S. C. Huckett, and B. I. Swanson, Phys. Rev. B **46**, 813 (1992).
[31]P. Dean, Proc. R. Soc. Ser. A **254**, 507 (1960).
[32]P. Dean, Proc. R. Soc. Ser. A **260**, 263 (1961).
[33]D. N. Payton and W. M. Visscher, Phys. Rev. **156**, 1032 (1967).
[34]W. M. Visscher and J. E. Gubernatis, in *Dynamical Properties of Solids,* edited by G. K. Horton and A. A. Maradudin (North-Holland, Amsterdam, 1980), Vol. 4.
[35]A. S. Barker and A. J. Sievers, Rev. Mod. Phys. **47**, Suppl. No. 2, S1 (1975).
[36]O. Bekaroglu, H. Breer, H. Endres, H. J. Keller, and H. N. Gung, Inorg. Chim. Acta **21**, 183 (1977).
[37]J. R. Campbell, R. J. Clark, and P. C. Turtle, Inorg. Chem. **17**, 3622 (1978).
[38]R. J. H. Clark and V. B. Croud, Inorg. Chem. **24**, 588 (1985).
[39]M. Tanaka and S. Kurita, J. Phys. C **19**, 3019 (1986).
[40]R. Ruppin and R. Englman, Rep. Prog. Phys. **33**, 149 (1970).
[41]L. Genzel and T. P. Martin, Surf. Sci. **34**, 33 (1973).
[42]B. Scott, R. J. Donohoe, S. P. Love, S. R. Johnson, M. P. Wilkerson, and B. I. Swanson, Synth. Met. (to be published).
[43]H. Okamoto, T. Mitani, K. Toriumi, and M. Yamashita, Mater. Sci. Eng. B **13**, L9 (1992).